

Dark-probe scanning near-field microscopy

Parsamyan, Henrik; Yezekyan, Torgom; Nerkararyan, Khachatur; Bozhevolnyi, Sergey I

Published in:
New Journal of Physics

DOI:
10.1088/1367-2630/acfdc5

Publication date:
2023

Document version:
Final published version

Document license:
CC BY

Citation for published version (APA):
Parsamyan, H., Yezekyan, T., Nerkararyan, K., & Bozhevolnyi, S. I. (2023). Dark-probe scanning near-field microscopy. *New Journal of Physics*, 25(10), Article 103015. <https://doi.org/10.1088/1367-2630/acfdc5>

Go to publication entry in University of Southern Denmark's Research Portal

Terms of use

This work is brought to you by the University of Southern Denmark.
Unless otherwise specified it has been shared according to the terms for self-archiving.
If no other license is stated, these terms apply:

- You may download this work for personal use only.
- You may not further distribute the material or use it for any profit-making activity or commercial gain
- You may freely distribute the URL identifying this open access version

If you believe that this document breaches copyright please contact us providing details and we will investigate your claim.
Please direct all enquiries to puresupport@bib.sdu.dk

PAPER • OPEN ACCESS

Dark-probe scanning near-field microscopy

To cite this article: Henrik Parsamyan *et al* 2023 *New J. Phys.* **25** 103015




View the [article online](#) for updates and enhancements.

You may also like

- [Scanning near-field optical microscopy system based on frequency-modulation atomic force microscopy using a piezoelectric cantilever](#)
Nobuo Satoh, Kei Kobayashi, Shunji Watanabe et al.
- [Temperature-dependent cathodoluminescence mapping of InGaN epitaxial layers with different In compositions](#)
Satoshi Kurai, Ayumu Wakamatsu and Yoichi Yamada
- [Fabrication of nanostructure on Au nano-film by nanosecond laser coupled with cantilevered scanning near-field optical microscopy probe](#)
Xuewen Wang, Jianlei Cui, Hailong Yin et al.



PAPER

Dark-probe scanning near-field microscopyHenrik Parsamyan^{1,2,*} , Torgom Yezekyan^{2,*} , Khachatur Nerkararyan¹  and Sergey I Bozhevolnyi² ¹ Institute of Physics, Yerevan State University, A. Manoogian 1, Yerevan 0025, Armenia² Centre for Nano Optics, University of Southern Denmark, Campusvej 55, DK-5230 Odense M, Denmark

* Authors to whom any correspondence should be addressed.

E-mail: hparsamyan@ysu.am and ty@mci.sdu.dk**Keywords:** anapole, scanning near-field optical microscopy, core-shell

OPEN ACCESS

RECEIVED
17 August 2023REVISED
21 September 2023ACCEPTED FOR PUBLICATION
27 September 2023PUBLISHED
11 October 2023Original content from
this work may be used
under the terms of the
[Creative Commons
Attribution 4.0 licence](https://creativecommons.org/licenses/by/4.0/).Any further distribution
of this work must
maintain attribution to
the author(s) and the title
of the work, journal
citation and DOI.**Abstract**

Scanning near-field optical microscopy (SNOM) is a well-known powerful optical technique for visualization of surface nanostructures and fields far beyond the diffraction limit and thus indispensable in material- and nanoscience. While the SNOM resolution is theoretically unlimited, the SNOM performance is in practice constrained by the signal-to-background ratio, simply because of light scattering scaling down as the sixth power of a nanoparticle size and useful signals rapidly drowning in the background for very small objects. In modern instruments, this problem is usually ameliorated through advanced post-processing techniques. Here, we suggest using, instead or in parallel, a ‘dark’ SNOM probe designed to suppress the background light scattering, so that the scattering occurs only when the probe is very close to a nanoscopic object. We argue and demonstrate with simulations that the dark-probe SNOM imaging is much more sensitive to the presence of tiny nanoparticles or any other nanoscale features, allowing thereby for superior resolution and sensing capabilities that are invaluable for nano-optical characterization.

1. Introduction

Optical imaging with high spatial resolution at the nanometer scale provides the path to the understanding of fundamental microscopic processes from the charge carrier dynamics in optical nanostructures to biological effects in cellular systems [1–4]. However, the resolution of a classical optical microscopy is generally limited by the diffraction to the half of the operating wavelength. To overcome this limitation, significant progress has been made over the past two decades through the development of various high-resolution techniques for optical characterization, including two-photon fluorescence microscopy [5], structured illumination microscopy [6], stimulated emission depletion microscopy [7], stochastic optical reconstruction microscopy [8] and scanning near-field optical microscopy (SNOM) [9]. Scattering-type SNOM (s-SNOM) is a particularly attractive technique with several unique advantages, including probing beyond the Abbe diffraction limit with wavelength-independent nanometer resolutions and polarization-, amplitude- and phase-resolved characterization of electromagnetic near-fields. These features combined make the s-SNOM one of the most powerful tools available for deterministic and non-destructive nano-optical characterization of electromagnetic properties of various nanostructures and materials [9–12].

The s-SNOM technique utilizes scattering of free-space propagating light by an atomic force microscope (AFM) probe tip placed in the vicinity of nanostructured objects. The AFM probe serves as an optical antenna to convert nanostructured near fields formed by probe-object interactions to the propagating away (towards a remote detector) far-field components. In addition, a sharp probe, which is usually made of metal-coated semiconductor (silicon Si) [13], provides strongly confined and enhanced electrical fields that interrogate the sample surface enabling thereby subwavelength resolution [14, 15]. The electric field confinement around the probe tip is determined by the curvature radius of the tip apex [16], which is of the order of 10–100 nm. The probe-confined and enhanced electrical fields generate useful signals through probe-sample interactions and scattering towards a remote detector. At the same time, the illuminated by the incoming laser beam area, being diffraction limited is significantly larger than the probe-sample interaction area. The scattered toward a detector light therefore contains not only useful signals but also the background

produced by scattering off the sample surface, cantilever and the probe tip itself [17]. Since useful signals generated by near-field probe-sample interactions are much weaker than the background, it is of crucial importance to accurately discriminate the signal from the background, a task that is usually dealt with by detecting high harmonics in the detected time-varying signals modulated by varying in time the probe-sample distance [9, 18]. However, for larger probes and smaller object features, the background level rapidly becomes dominant even in high harmonics, rendering near-field signal contributions scrambled and nanostructured object features indistinguishable.

A similar problem exists also in the domain of classical optical microscopy: very small or low-contrast features are often difficult to distinguish on a bright background created by a transmitted or reflected light. This problem is solved by blocking the directly transmitted or specular reflected, i.e. unscattered, optical fields. The corresponding technique, dark-field microscopy, results in images that are generally dark with bright sample features clearly discernible. Inspired by this classical approach, we started looking for ways to suppress strong background light scattering, quickly realizing that, in the context of near-field microscopy, this means to employ a probe that does not scatter incident (illuminating) light when being away from a sample surface, i.e. to employ a 'dark' probe. We considered a probe tip to be represented by a small sphere, which is widely used to estimate the scattering cross-section in s-SNOM [9, 19, 20]. A promising strategy to achieve a non-scattering probe is to utilize a dielectric core coated with a metallic shell. The core-shell (C-Sh) particles (with nm-thin shells) have been introduced more than 20 years ago [21] and used for numerous practical applications [22, 23]. Since the local polarization vectors of the dielectric core and metallic shell have opposite signs, the two electric dipole moments can cancel each other, nullifying a dipolar polarizability and thus strongly reducing the light scattering by such a C-Sh particle [24]. We have however realized that this approach is not practical because of being valid only within the limits of the quasistatic approximation when the size of the particle is much smaller than the incident light wavelength [25]. A more general approach should involve the multipolar engineering [26]. While being negligible in homogeneous or small (compared with the effective wavelength) particles, the interaction between the toroidal and Cartesian moments may become crucial in high refractive index dielectric or hybrid C-Sh particles [27, 28]. The destructive interference between the toroidal and Cartesian multipoles leads to the emergence of the so-called optical anapole states, which are characterized by strongly suppressed far-field scattering [28, 29].

Here, we introduce a dark probe s-SNOM approach involving the use of a Si-core Au-shell particle designed to operate in an anapole state, which is achieved by identifying the core radius and shell thickness corresponding to the operating wavelength. A three-dimensional full-wave numerical finite element method-based analysis has been conducted to calculate the optical response of the Si, Au and Si-Au C-Sh probes, revealing the peculiarities of their interaction with metallic and high-index dielectric nanosized objects. We show that the dark C-Sh probe provides improved interaction with both dielectric and metallic objects compared with homogeneous dielectric and metallic probes. Moreover, by considering the detection of only forward scattered waves instead of all scattered ones and using radially polarized illumination, one can further improve the spatial resolution and contrast in the dark-probe SNOM imaging.

2. Probe-object configuration and simulation details

The geometry of the probe-object configuration is illustrated in figure 1(a), where a section of a C-Sh particle is removed to show the internal structure; the object is represented as a small sphere and the scanning is performed in the XY plane. The particle is composed of a Si core with a radius of 100 nm covered by a 10 nm thick Au shell. The core radius is chosen close to the real-life s-SNOM tip apex radius, while the shell size was chosen to tune the anapole state to maintain in the near-infrared region. The simulation model comprises a C-Sh probe positioned at the center of the coordinate system and surrounded by a concentric sphere whose radius is larger than the incident wavelength. The entire system is enclosed by a perfectly matched layer intended to imitate a free space by eliminating the back-scattering of electromagnetic waves. The so-called scattered field formulation of commercial COMSOL Multiphysics software was used to properly calculate the scattered field produced by an object placed in the incident background field. We first show the total scattering efficiency (scattering cross-section normalized to the geometrical cross-section) of the C-Sh particle (black line) and compare it with a pure Si and Au spheres (blue and red lines, respectively) (figure 1(b)). The Si particle has a radius of 100 nm (identical to the core of the C-Sh), and the radius of the Au particle is 110 nm. The material properties (refractive indices) of Si and Au were exploited from [30] and [31] respectively and the ambient medium of a particle is air. One notices a well pronounced deep minimum in the scattering spectrum of the C-Sh particle at the wavelength of 1320 nm, where the scattering is nearly one order of magnitude smaller than from the homogeneous Si sphere.

This wavelength corresponds to the first anapole state of the C-Sh particle, i.e. the destructive interference between electric and toroidal dipole moments [32]. Another minimum in the scattering of the Si

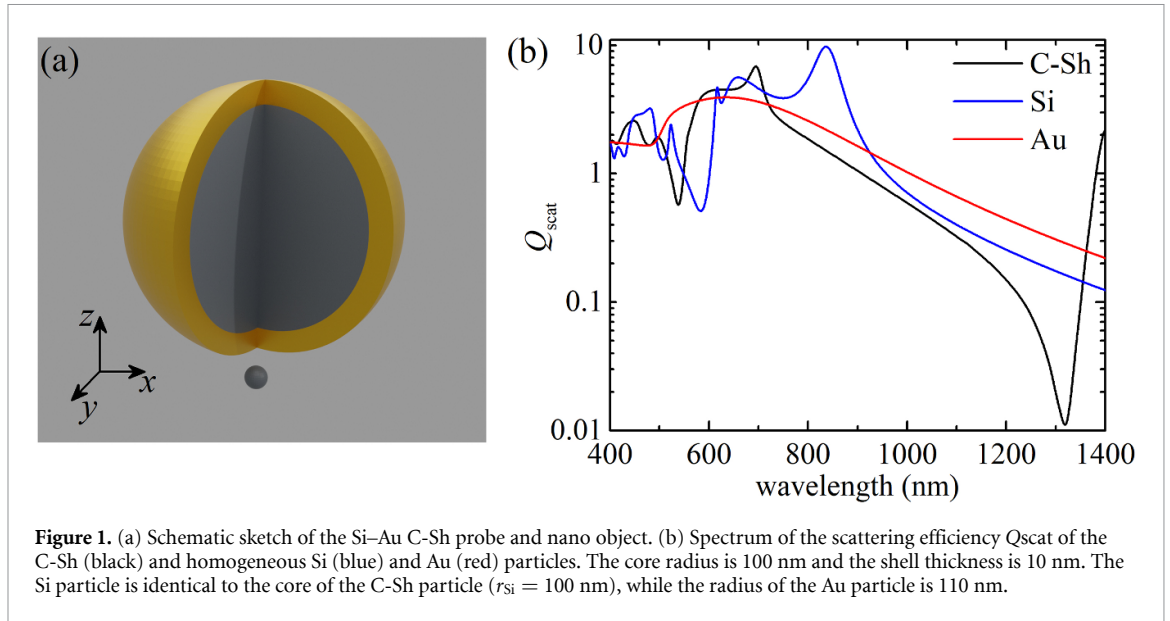


Figure 1. (a) Schematic sketch of the Si–Au C-Sh probe and nano object. (b) Spectrum of the scattering efficiency Q_{scat} of the C-Sh (black) and homogeneous Si (blue) and Au (red) particles. The core radius is 100 nm and the shell thickness is 10 nm. The Si particle is identical to the core of the C-Sh particle ($r_{\text{Si}} = 100$ nm), while the radius of the Au particle is 110 nm.

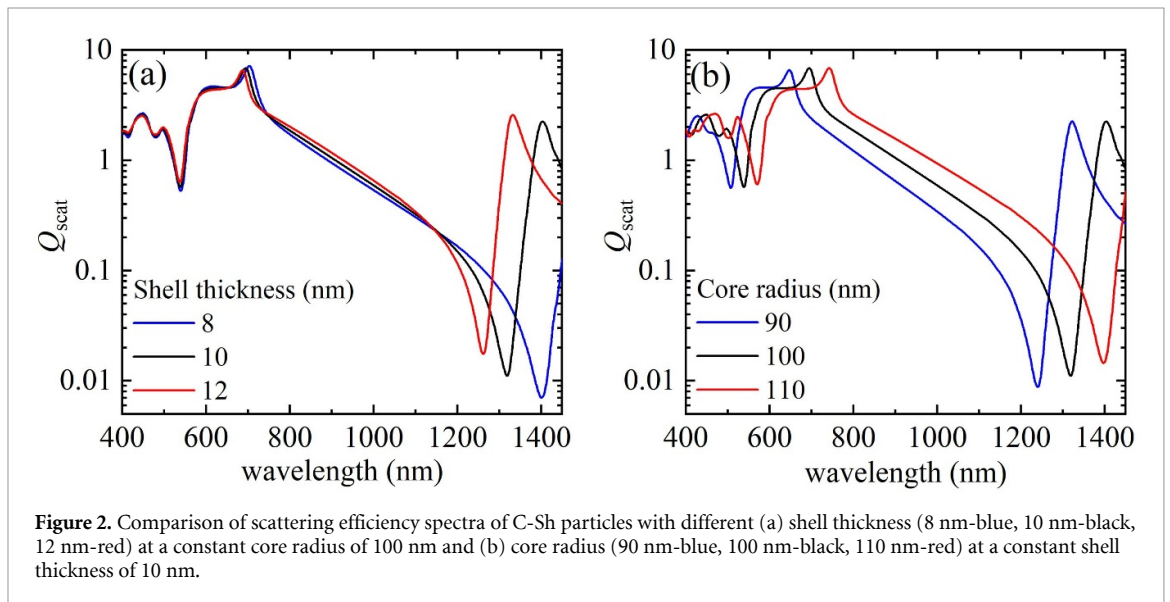


Figure 2. Comparison of scattering efficiency spectra of C-Sh particles with different (a) shell thickness (8 nm-blue, 10 nm-black, 12 nm-red) at a constant core radius of 100 nm and (b) core radius (90 nm-blue, 100 nm-black, 110 nm-red) at a constant shell thickness of 10 nm.

sphere is seen at the wavelength of 584 nm (figure 1(b)). The reason for this is the fact that the high refractive index particles having a radius of the same order as the effective wavelength inside the particle may support both electric and toroidal higher order modes, resulting in the formation of anapole states in this material [33]. However, in this case, the scattering efficiency does not decrease as strongly as for the C-Sh particle due to the contribution of other multipoles to the total scattering [34]. The main advantage of using C-Sh probes is that the anapole wavelength can be engineered by adjusting the shell thickness.

The anapole state in the hybrid C-Sh particles is noticeably influenced by the geometrical sizes, such as core radius and shell thickness. For a quick estimation of the resonance tunability, one can use, as a guideline, the electrostatic scaling rule for nm-size C-Sh particles, for which only the ratio between the core radius and shell thickness is important. Indeed, our accurate simulations show that the position of the anapole state of the C-Sh probe blueshifts as the shell thickness increases and/or the core radius decreases. Thus, the anapole wavelength of C-Sh probes with the 8, 10 and 12 nm thick shells, while the core radius is kept at 100 nm, decreases from 1401 nm, to 1320 and 1263 nm, respectively (figure 2(a)). Concomitantly, decreasing the core radius in steps of 10 nm from that equal to 110 nm, while the shell thickness is kept at 10 nm, introduces a similar blueshift in the anapole wavelength, which decreases from 1396 nm to 1320 and 1240 nm, respectively (figure 2(b)). Therefore, the anapole position and hence the scanning wavelength can efficiently be engineered by the corresponding choice of the shell thickness and core radius, enabling thereby the investigation of various nano objects at different wavelengths.

It is worth mentioning that the suppression of a certain multipole (dipole moment in our case) may not lead to strong scattering suppression, if the contribution of other multipoles is considerably large. The typical way of suppressing the undesired multipoles is to modify the geometry of the particle, for example, the shift from a dielectric sphere to a disk, suppresses the magnetic dipole moment in it because a thin dielectric slab supports only a transverse electromagnetic (TEM) mode with in-plane electric and out-of-plane magnetic fields [33, 35, 36]. This can also be done by using non-homogeneous illumination, particularly a focused radially polarized beam, which generates strong longitudinal polarization in the focus.

We further proceed with the analysis of the probe-object interactions assuming that (i) at the initial position, the 110 nm radius probe is placed at the origin of the coordinate system and the object is below the probe such that the separation gap between their surfaces is 1 nm along the z -axis; and (ii) the probe is illuminated by a radially polarized electro-magnetic wave propagating along the $-z$ direction [37].

3. Dark-probe SNOM imaging

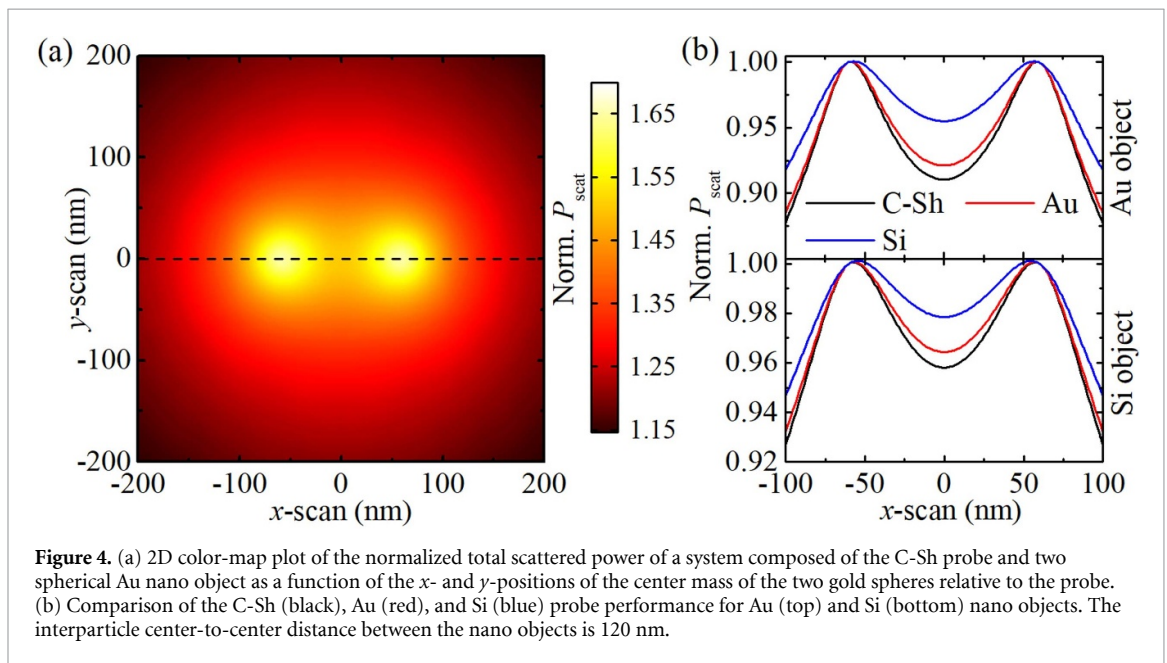
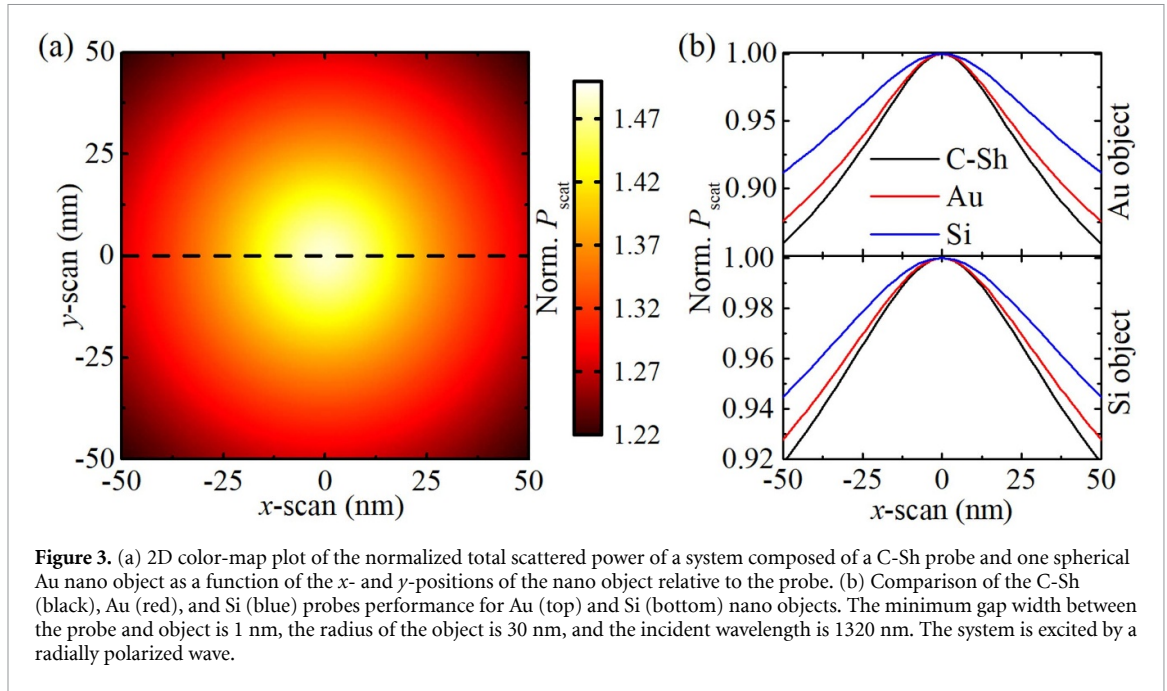
The dark-probe SNOM imaging was investigated by considering the C-Sh probe under the radially polarized illumination at the wavelength of 1320 nm, corresponding to the probe anapole state. We computed two-dimensional (2D) maps of the normalized scattered power as a function of the object position in the XY plane in figure 3(a). The object is an Au (Si) sphere with a radius of 30 nm. It should be noted that the object material is expected to be of secondary importance, influencing only the degree of near-field perturbation. Si and Au were chosen as nano object materials to demonstrate the possibilities of resolving high-index dielectric and metal objects (representing two extreme cases with respect to the dielectric susceptibility) with the proposed C-Sh dark probe. Hereinafter, the scale bars of all 2D plots are normalized to the total scattered power of the isolated object and probe. It is seen that the interaction between the probe and object is the strongest when the probe is directly above the object, producing about 1.5-fold enhancement of the scattered power compared to that produced by the isolated probe (figure 3).

When operating at $\lambda = 1320$ nm, the C-Sh particle is not expected to scatter electromagnetic fields (figure 1(b)), however moving the object close to the probe causes distortion of the anapole state of the probe such that the dipole and toroidal moments do not cancel each other anymore, resulting in an increased scattering of the probe-object system. Figure (b) shows the spatial variations of the normalized scattered powers for a C-Sh (black), Au (red) or Si (blue) probes (all having the same external diameter) and Au (top) and Si (bottom) nanospheres as an object, when conducting a linear scan along the x -axis (the cutline is marked with a dashed line in figure 3(a)). Hereinafter all the linear plots are normalized to their peak value, to be able to juxtapose the signals from different probes. It is seen that, for both nano objects, the C-Sh probe demonstrates the best imaging performance, providing the smallest images of both Au and Si nanospheres.

To investigate the spatial resolution improvement when imaging with the C-Sh probe, we calculated the scattered power in the XY -plane for different probes scanning over two identical Au nanospheres with a radius of 30 nm and interparticle center-to-center distance of 120 nm (figure 4). The scattered power contrast between the positions when the probe is right above one of the objects and at the furthest distance in the XY -plane is improved compared with that of one nano object.

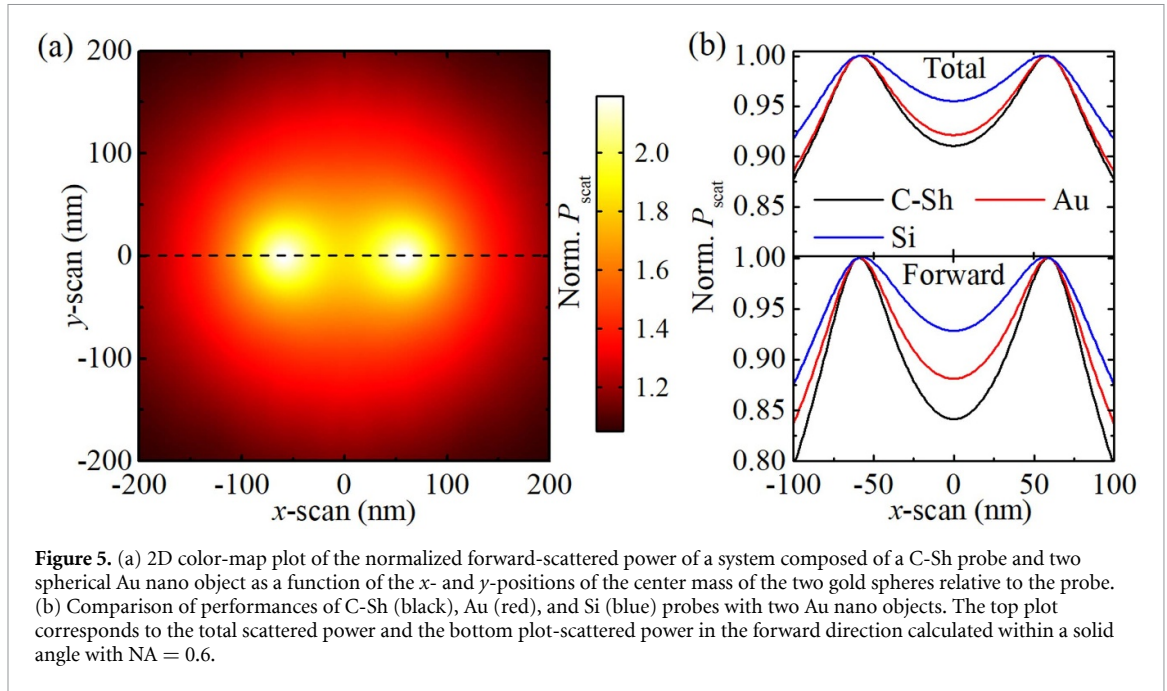
As in the previous consideration (figure 3(b)), the imaging of two objects with different probes (Au, Si and C-Sh) being scanned over either Au (top plot) or Si (bottom plot) object nanospheres is compared in figure 4(b). Two bright spots with enhanced signals are observed in the calculated images (figure 4(a)) corresponding to the position of the probe right above each of the nano objects, with sufficiently pronounced dips seen when the C-Sh probe passes over the center of the object separation with the normalized scattered power decreasing to ~ 0.91 for Au and ~ 0.96 for Si object nanoparticles. For both metallic and high-index dielectric object compositions, the contrast observed in the scattering SNOM images is noticeably improved when using the C-Sh probe. Such a contrast would allow one to safely resolve these nano objects, whose sizes (60 nm in diameter) are considerably smaller (>3 times) than that of the 220 nm diameter C-Sh probe.

Depending on the incident beam direction and the detection scheme, two s-SNOM modes are categorized: oblique incidence mode and transmission mode. In the first mode the exciting laser, tip and collecting optics with the detector are placed above the sample and the non-transparent substrate, and the signal reflected (scattered) from the sample is detected and eventually analyzed. On the other hand, the transmission-mode detection scheme exploits forward scattered signals to retrieve the amplitude-phase distribution of a nanostructure [13, 38]. Here, however, the optically transparent substrates at exciting wavelengths of the SNOM tip need to be employed. The analysis above shows the dependence of the normalized total scattered power on the relative position of the probe-objects, where the scattered power in all scenarios was calculated over a spherical surface enclosing the entire system. The operation of the suggested s-SNOM system in the transmission mode, when the forward-scattered signal from the nano object is used for near-field analysis is demonstrated in figure 5. Since, in this configuration for collecting the



signal, long working distance objectives are used (there should be some space left for the tip), we calculated the forward-scattered power within a solid angle in the illumination direction corresponding to a typical numerical aperture (NA) of 0.6. Figure 5(a) shows the 2D map of the normalized forward-scattered power dependence on the probe position in respect to the two identical gold nanospheres in the XY plane. The sizes of nanoparticles, as well as their distance are as in figure 4.

Normalization, in this case, is performed by the sum of powers scattered from the isolated probe and nano objects in the forward direction within the solid angle with $NA = 0.6$. One can note that the maximum value of the normalized power in forward direction (~ 2.2) is larger than the total scattered power (~ 1.6) and the power contrast between the peak values (when the probe is right above a nanoparticle) and the central dip (when the probe is right above the center of mass of nanoparticles) is noticeably improved. It is also seen in figure 5(b), comparing the dependence of the normalized total (top) and forward-scattered (bottom) powers on the position of the probe along x -axis (dashed horizontal line in figure 5(a)) considering Au, Si and C-Sh probes, and Au nano objects. The normalized total scattered signal corresponding to the probe position above the center mass of nano objects is 0.91 in respect to the peak value, whereas that for the forward-scattered power is 0.84.



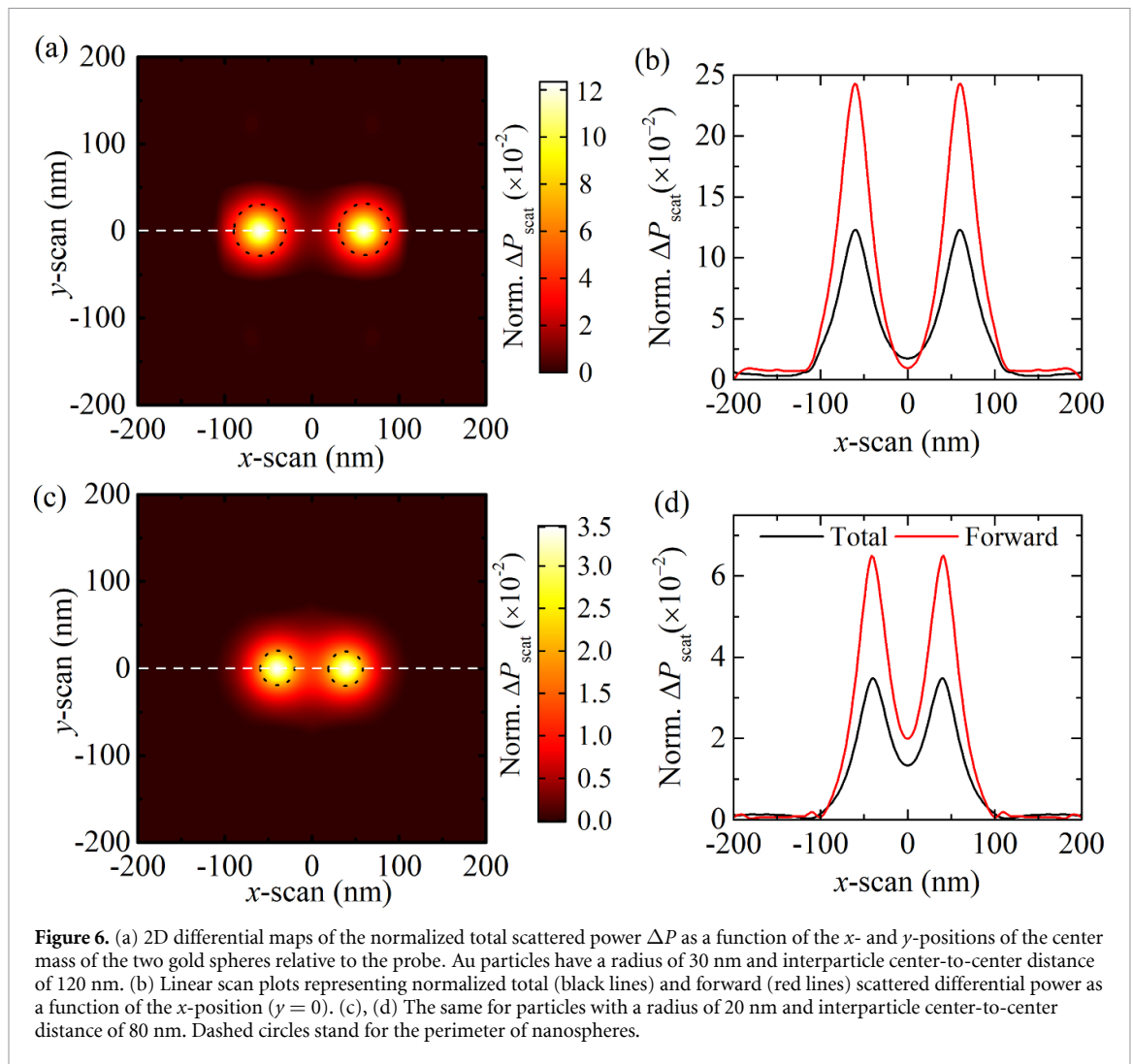
4. Differential dark-probe SNOM imaging

Similarly, to the s-SNOM, the contrast in the scattered power map can significantly be enhanced by subtracting the maps obtained at different distances between the probe and nano objects (figure 6). Here the differential power was derived as follows: first the scan in the XY plane was performed at the minimum (1 nm) distance between the probe and nano objects planes. Then the distance is increased to 5 nm and the final image was computed via point-by-point subtraction of the normalized scattered powers:

$$\text{Norm}\Delta P_{\text{scat}} = P_1(x, y, z_1) - P_2(x, y, z_2), \quad (1)$$

where P_1 corresponds to the normalized scattered power of the system with the minimum distance between surfaces of the object and probe of 1 nm, and P_2 —with the minimum distance of 5 nm. Recall that both P_1 and P_2 are normalized via the total scattered power of the isolated probe and nano objects. The proposed method for obtaining differential maps is essentially a first-order approximation of the demodulation process employed in the conventional s-SNOM, representing thereby the numerical implementation of its tapping mode operation. Figure 6(a) shows 2D differential map of the normalized total scattered power $\text{Norm}\Delta P_{\text{scat}}$ of two identical Au particles with a radius of 30 nm and interparticle center-to-center distance of 120 nm; and (b) plots the dependence of the total (black line) and forward (red line) scattered differential power on the x -position of the center mass of nano objects. Dashed circles in (a) stand for the perimeter of nanospheres. The scattered differential signal is practically zero in the regions around the nanoparticles as particles do not interact with the probe and hence varying the distance does not alter the scattered signal. Moreover, a large contrast between peaks and the central dip is also achieved in this case with the differential power approaching zero at the center of the interparticle gap thus making the hotspots clearly resolved.

Here again, the operation based on the transmission mode provides a higher normalized scattered signal in the forward direction compared with the total scattered power. The full width at half-maximum of the $\Delta P_{\text{scat}}(x)$ curve is about 42 nm and 45 nm for the forward and total scattered differential signals, respectively. To demonstrate the imaging performance of a C-Sh dark-probe with smaller objects, we considered nanoparticles having a radius of 20 nm and interparticle center-to-center distance of 80 nm. The results are shown in figures 6(c) and (d) in a similar manner as for 30 nm radius particles. One can see that unlike the case of larger particles, here the differential signal in the region between the particles did not vanish; and the contrast between the peak and central dip values of the differential scattered power is not as pronounced as for larger particles. The main reason for this is that when the distance between a 110 nm radius probe and 20 nm radius spheres is increased, the probe-nano object interaction is weakened due to their small sizes and interparticle distance. As a result, the two maxima of normalized $P_{\text{scat}}(x)$ corresponding to the probe position above each nanosphere are hardly distinguishable; and the contrast is not effectively improved. However, the peak-to-dip depths are nearly 4.5 and 2.15 for the total and forward-scattered powers,



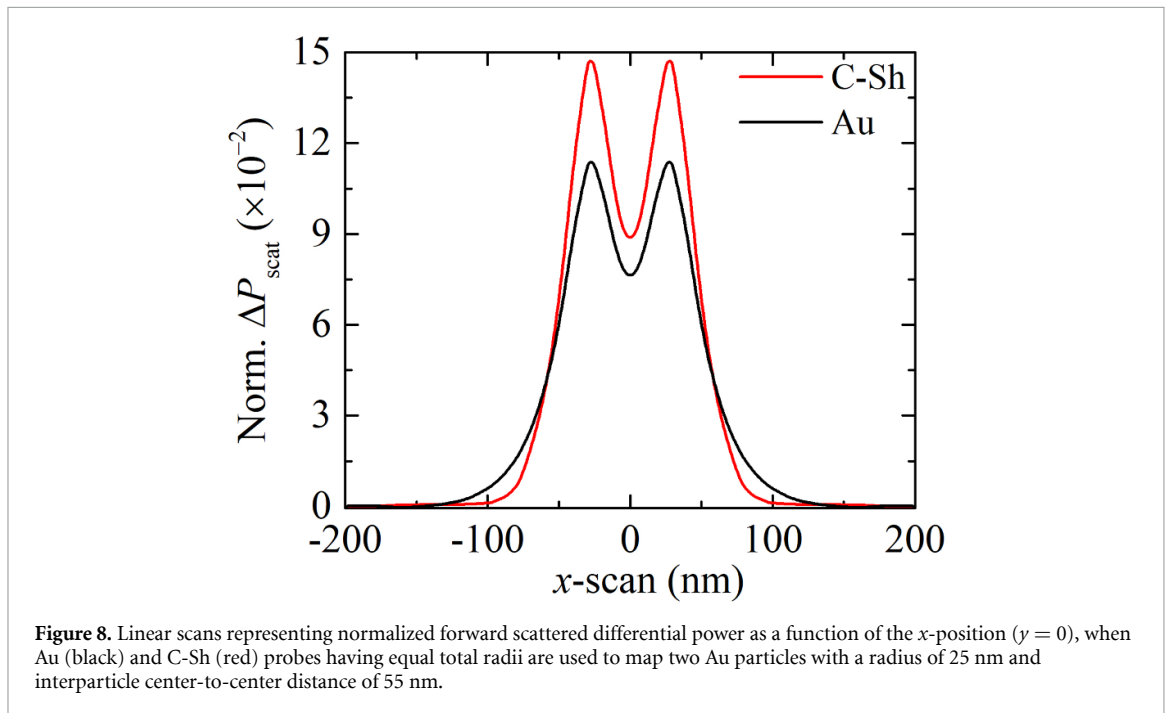
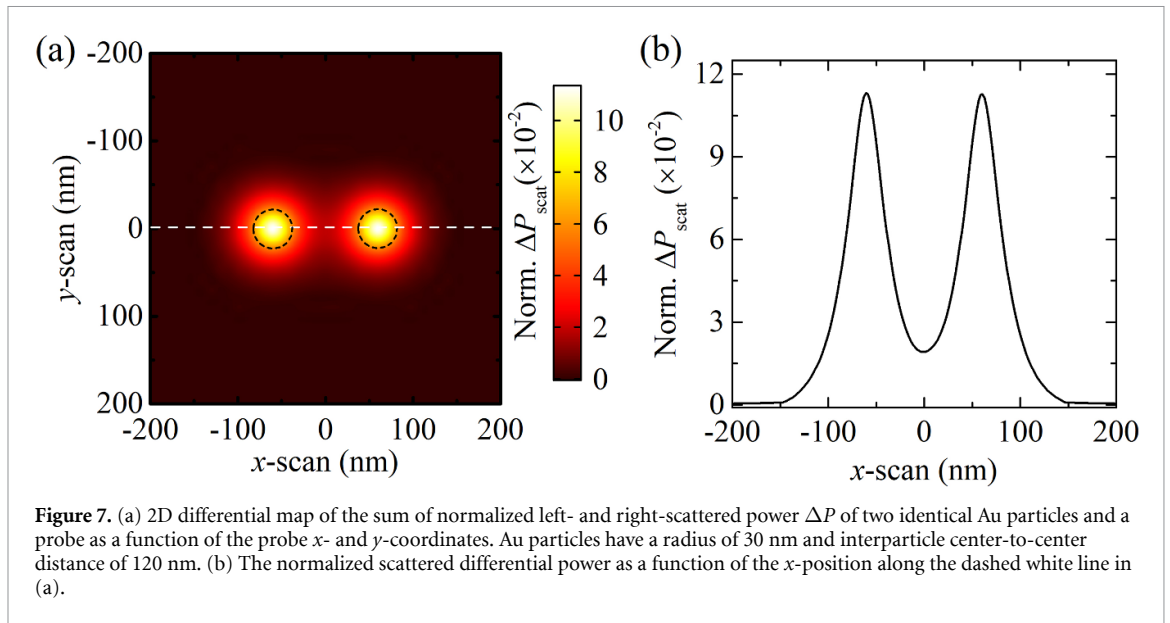
respectively, and the two distinct hot spots are still clearly distinguishable. For comparison, those for above-considered larger particles (with 30 nm radii) are about 23.4 and 10.6 for the.

One of the widely employed s-SNOM experimental schemes is based on the detection and analysis of the reflected (scattered) signal from the samples under test distributed on an opaque substrate. In this case, the back- or forward-scattered signal can be collected by side lenses. To show the operation according to this scheme, the scattered power was calculated within two solid angles corresponding to $NA = 0.6$ positioned on the left- and right-hand sides of the probe (with the base being parallel to the XZ -plane, the z -axis being parallel to the propagation direction of the exciting beam and nano objects being separated along the x -axis).

The results of the scan, i.e. 2D differential image of the sum of normalized left- and right-scattered power of two identical Au particles (with the dimensions as in figure 6(a)) are shown in figure 7(a), while figure 7(b) shows the differential power as a function of the probe position along the x -axis (white dashed line in figure (a)). Two hot spots in the differential power map are clearly resolved with a peak-to-dip depth of about 9.4. Hence, the suggested C-Sh probe can be used for electric near-field mapping of nano objects distributed on either optically transparent or opaque substrates, where forward- or side-scattered signals are to be analyzed.

Finally, to compare the resolving performance of the proposed C-Sh probe with that of a widely used homogeneous metallic probe, we calculated the linear scans of two 25 nm radius Au object nanospheres performed with the 'dark' C-Sh and Au probes of equal total radii of 110 nm (figure 8).

The center-to-center distance of 55 nm was chosen to better test the resolution of SNOM imaging. It is seen that the peak-to-dip depth of the normalized forward-scattered differential power in the case of the C-Sh probe is about 5.8, whereas that of the Au probe is only 3.6, justifying the superior resolution of the dark-probe s-SNOM.



5. Discussion and conclusion

In this work we have introduced a conceptually novel s-SNOM operation mode, a dark-probe s-SNOM, which is based on using a specially designed SNOM probe whose scattering is strongly suppressed when the illuminated probe is away from nanostructures to be inspected. With the background light scattering being suppressed, the efficient light scattering occurs only when the probe is very close to a nanoscopic object. We have argued that the dark-probe SNOM imaging should be much more sensitive to the presence of tiny nanoparticles or any other nanoscale features, allowing thereby for superior resolution and sensing capabilities. We have further suggested that the probe should be designed to operate in an anapole state and considered the suitably devised Si-core Au-shell 110 nm radius spherical probe operating at 1320 nm. We should note that, although the ‘dark’ state of a probe is achieved only within a narrow bandwidth, the dark-probe s-SNOM can be used in applications where the wavelength variation is not required, such as mapping near fields of optical waveguides. Also, to operate at different wavelengths, different C-Sh probes with different core radii or shell thicknesses can easily be designed as described in our work. We would like to further note that although a practical SNOM probe is not necessarily spherical and usually connected to a

macroscopic trunk contributing to the background scattering, the simplified configuration considered is useful to reveal the underlying physical mechanisms at play in the s-SNOM. Furthermore, there have been described numerous SNOM configurations, including those using an isolated small particle positioned with the help of optical tweezers in aqueous solutions [39] or being attached to the apex of low-index (fiber) probe [40]. These SNOM configurations are very closely related to that we considered in the present work. In general, one can attempt implementing the idea of a ‘dark’ probe in any practical s-SNOM configuration (i.e. for given probe materials and shapes involved along with given illumination and detection arrangements) by tuning the probe geometry and material composition to a minimum of background scattering. We also want to mention that the creation of anapole state was reported for a truncated conical structure of an arbitrary size [41], highlighting the possibility of creation of anapole states in geometries that are lacking spherical symmetry. In this context the combination of a conical structure with C-Sh particle will simply increase the tunability of the anapole state. It is expected that the results presented in our work can also be useful in this general case by highlighting important matters, such as the influence of polarization and detection direction.

A three-dimensional full-wave numerical finite element method-based analysis has been conducted to calculate the optical response of the Si, Au and Si–Au C-Sh probes, revealing the peculiarities of their interaction with metallic and high-index dielectric nanosized objects. We have shown that the dark C-Sh probe provides improved interaction with both dielectric and metallic objects compared with homogeneous dielectric and metallic probes. Moreover, by considering the detection of only forward scattered waves instead of all scattered ones and using radially polarized illumination, we have demonstrated that one can further improve the spatial resolution and contrast in the dark-probe SNOM imaging and thereby resolve nano objects that are much smaller and closer than the probe size. We believe that the suggested dark-probe SNOM operation may find various applications, especially when dealing with complicated matters, and turned out being invaluable for nano-optical characterization.

Data availability statement

All data that support the findings of this study are included within the article (and any supplementary files).

Acknowledgments

This work was supported by the Scientific Research Grant through the State Committee of Science of Ministry of Education, Science, Culture and Sports of Armenia (21AG-1C061).

ORCID iDs

Henrik Parsamyan  <https://orcid.org/0000-0003-4211-2978>
Torgom Yezekyan  <https://orcid.org/0000-0003-2019-2225>
Khachatur Nerkararyan  <https://orcid.org/0000-0001-7171-4113>
Sergey I Bozhevolya  <https://orcid.org/0000-0002-0393-4859>

References

- [1] Narimanov E 2019 Resolution limit of label-free far-field microscopy *Adv. Photon.* **1** 1
- [2] Ingham J et al 2018 An evaluation of the application of the aperture infrared SNOM technique to biomedical imaging *Biomed. Phys. Eng. Express* **4** 025011
- [3] Pohl D W, Denk W and Lanz M 1984 Optical stethoscopy: image recording with resolution $\lambda/20$ *Appl. Phys. Lett.* **44** 651–3
- [4] Lewis A, Isaacson M, Harootunian A and Muray A 1984 Development of a 500 Å spatial resolution light microscope *Ultramicroscopy* **13** 227–31
- [5] Yeh C-H, Tan C-Z, Cheng C A, Hung J-T and Chen S-Y 2018 Improving resolution of second harmonic generation microscopy via scanning structured illumination *Biomed. Opt. Express* **9** 6081
- [6] Heintzmann R and Huser T 2017 Super-resolution structured illumination microscopy *Chem. Rev.* **117** 13890–908
- [7] Blom H and Widengren J 2017 Stimulated emission depletion microscopy *Chem. Rev.* **117** 7377–427
- [8] Tam J and Merino D 2015 Stochastic optical reconstruction microscopy (STORM) in comparison with stimulated emission depletion (STED) and other imaging methods *J. Neurochem.* **135** 643–58
- [9] Chen X, Hu D, Mescall R, You G, Basov D N, Dai Q and Liu M 2019 Modern scattering-type scanning near-field optical microscopy for advanced material research *Adv. Mater.* **31** 1804774
- [10] Heydarian H, Shahmansouri A, Yazdanfar P and Rashidian B 2018 Dual-color plasmonic probes for improvement of scanning near-field optical microscopy *J. Opt. Soc. Am. B* **35** 627
- [11] Gadalla M N, Chaudhary K, Zgrabik C M, Capasso F and Hu E L 2020 Imaging of surface plasmon polaritons in low-loss highly metallic titanium nitride thin films in visible and infrared regimes *Opt. Express* **28** 14536
- [12] Huang J, Cui T, Sun J-L, Bai B and Sun H-B 2022 Super-resolved discrimination of nanoscale defects in low-dimensional materials by near-field photoluminescence spectral imaging *Opt. Lett.* **47** 4227

- [13] Duan J, Li Y, Zhou Y, Cheng Y and Chen J 2019 Near-field optics on flatland: from noble metals to van der Waals materials *Adv. Phys. X* **4** 1593051
- [14] Centrone A 2015 Infrared imaging and spectroscopy beyond the diffraction limit *Annu. Rev. Anal. Chem.* **8** 101–26
- [15] Achmari P, Siddiquee A M, Si G, Lin J, Abbey B and Kou S 2021 Investigating the probe-tip influence on imaging using scanning near-field optical microscopy *OSA Contin.* **4** 1143
- [16] Pors A, Nerkararyan K V and Bozhevolnyi S I 2014 Scaling in light scattering by sharp conical metal tips *Opt. Lett.* **39** 3308
- [17] Atkin J M, Berweger S, Jones A C and Raschke M B 2012 Nano-optical imaging and spectroscopy of order, phases, and domains in complex solids *Adv. Phys.* **61** 745–842
- [18] Yao Z, Xu S, Hu D, Chen X, Dai Q and Liu M 2020 Nanoimaging and nanospectroscopy of polaritons with time resolved s-SNOM *Adv. Opt. Mater.* **8** 1901042
- [19] Aminpour H, Eng L M and Kehr S C 2020 Spatially confined vector fields at material-induced resonances in near-field-coupled systems *Opt. Express* **28** 32316
- [20] Knoll B and Keilmann F 2000 Enhanced dielectric contrast in scattering-type scanning near-field optical microscopy *Opt. Commun.* **182** 321–8
- [21] Prodan E, Radloff C, Halas N J and Nordlander P 2003 A hybridization model for the plasmon response of complex nanostructures *Science* **302** 419–22
- [22] Halas N J, Lal S, Link S, Chang W, Natelson D, Hafner J H and Nordlander P 2012 A plethora of plasmonics from the laboratory for nanophotonics at Rice University *Adv. Mater.* **24** 4842–77
- [23] Kristensen A, Yang J K W, Bozhevolnyi S I, Link S, Nordlander P, Halas N J and Mortensen N A 2016 Plasmonic colour generation *Nat. Rev. Mater.* **2** 16088
- [24] Alù A and Engheta N 2005 Achieving transparency with plasmonic and metamaterial coatings *Phys. Rev. E* **72** 016623
- [25] Kerker M 1982 Lorenz–Mie scattering by spheres: some newly recognized phenomena *Aerosol Sci. Technol.* **1** 275–91
- [26] Liu W and Kivshar Y S 2017 Multipolar interference effects in nanophotonics *Phil. Trans. R. Soc. A* **375** 20160317
- [27] Colom R, McPhedran R, Stout B and Bonod N 2019 Modal analysis of anapoles, internal fields, and Fano resonances in dielectric particles *J. Opt. Soc. Am. B* **36** 2052
- [28] Yang Y and Bozhevolnyi S I 2019 Nonradiating anapole states in nanophotonics: from fundamentals to applications *Nanotechnology* **30** 204001
- [29] Baryshnikova K V, Smirnova D A, Luk'yanchuk B S and Kivshar Y S 2019 Optical anapoles: concepts and applications *Adv. Opt. Mater.* **7** 1801350
- [30] Green M A 2008 Self-consistent optical parameters of intrinsic silicon at 300K including temperature coefficients *Sol. Energy Mater. Sol. Cells* **92** 1305–10
- [31] McPeak K M, Jayanti S V, Kress S J P, Meyer S, Iotti S, Rossinelli A and Norris D J 2015 Plasmonic films can easily be better: rules and recipes *ACS Photonics* **2** 326–33
- [32] Liu W, Zhang J and Miroshnichenko A E 2015 Toroidal dipole-induced transparency in core-shell nanoparticles *Laser Photon. Rev.* **9** 564–70
- [33] Miroshnichenko A E, Evlyukhin A B, Yu Y F, Bakker R M, Chipouline A, Kuznetsov A I, Luk'yanchuk B, Chichkov B N and Kivshar Y S 2015 Nonradiating anapole modes in dielectric nanoparticles *Nat. Commun.* **6** 8069
- [34] Ladutenko K, Pal U, Rivera A and Peña-Rodríguez O 2017 Mie calculation of electromagnetic near-field for a multilayered sphere *Comput. Phys. Commun.* **214** 225–30
- [35] Zenin V A, Evlyukhin A B, Novikov S M, Yang Y, Malureanu R, Lavrinenko A V, Chichkov B N and Bozhevolnyi S I 2017 Direct amplitude-phase near-field observation of higher-order anapole states *Nano Lett.* **17** 7152–9
- [36] Yang Y, Zenin V A and Bozhevolnyi S I 2018 Anapole-assisted strong field enhancement in individual all-dielectric nanostructures *ACS Photonics* **5** 1960–6
- [37] Novotny L and Hecht B 2012 *Principles of Nano-Optics* (Cambridge University Press)
- [38] Schnell M, Garcia-Etxarri A, Huber A J, Crozier K B, Borisov A, Aizpurua J and Hillenbrand R 2010 Amplitude- and phase-resolved near-field mapping of infrared antenna modes by transmission-mode scattering-type near-field microscopy *J. Phys. Chem. C* **114** 7341–5
- [39] Prikulis J, Svedberg F, Käll M, Enger J, Ramser K, Goksör M and Hanstorp D 2004 Optical spectroscopy of single trapped metal nanoparticles in solution *Nano Lett.* **4** 115–8
- [40] Sqalli O, Utker I, Hoffmann P and Marquis-Weible F 2002 Gold elliptical nanoantennas as probes for near field optical microscopy *J. Appl. Phys.* **92** 1078–83
- [41] Kuznetsov A V, Canós Valero A, Shamkhi H K, Terekhov P, Ni X, Bobrovs V, Rybin M V and Shalin A S 2022 Special scattering regimes for conical all-dielectric nanoparticles *Sci. Rep.* **12** 21904